Smart Grid Connection of an Induction Motor Using a Three-Phase Floating H-bridge System as a Series Compensator

Siyu Leng, *Member, IEEE*, A. R. N. M. Reaz Haque, Nirmana Perera, Andrew M. Knight, *Senior Member, IEEE*, and John Salmon, *Member, IEEE*

***Abstract*—Electrical grid voltage sags are a significant industrial power quality concern. According to a survey result across the US, voltage sags and short-duration power outages are responsible for 92% of power quality problems faced by industrial customers. These power interruptions often impose severe cost penalties in plant shutdowns for many industries. A series compensation scheme for an induction motor is presented with inherent voltage sag ride through capability. The system utilizes a system of three-phase floating capacitor H-bridge converters located in each phase between the utility grid and a squirrel-cage induction motor. By injecting a series voltage in each phase, the proposed system can manipulate the voltage supplied to a motor, increasing its tolerance of grid voltage sags. The voltage injection scheme has an inherently leading grid power factor under steady state and, hence, generates VARs into the grid, over a wide range of load conditions. The paper develops mathematical analysis of the proposed system to quantify both the voltage sag ride-through and the reactive power generation that results. The analysis shows that voltage sag tolerance of the proposed system is closely related to the motor fundamental power factor. Moreover, it is found that unity power factor operation of the system, as seen from the grid, is possible and that the reactive power generation capability can also be accurately quantified. A 5-hp experimental testbed is used to validate both the grid voltage ride-through capability feature and the reactive power generation characteristics.**

***Index Terms*—Floating capacitor, H-bridge converters, induction motor, reactive power generation, series compensation, voltage sag ride-through.**

I. Introduction

INDUCTION motors (IMs) are one of the most commonly used pieces of industrial electrical equipment, with wide ranging applications [1]–[3]. In fact, more than 90% of industrial electrical motors are three-phase squirrel-cage induction motors [4]. In practice, depending on application requirements, induction motor can be either directly connected to the grid or connected through a variable-frequency drive (VFD). When directly grid connected, induction motors (and the industrial processes they drive) are one of the industrial components that are more sensitive to voltage disturbances [5]. With an incidence between 61% and 87%, voltage sags are the main cause of voltage disturbances in industrial systems [6]. Voltage sags are normally caused by faults on the power system but can also be caused by energizing of heavy loads or starting of large motors. A survey of over 2000 events in the US found that the majority of voltage sags had a magnitude of around 80% of rated voltage and duration of less than seven cycles [7]. When induction motor terminal is directly subjected to voltage sag, the motor current can increase significantly and large mechanical torques may occur that cause damage to the motor shaft or equipment connected to the shaft. In addition, inrush current at the instant of voltage recovery may trip overcurrent protection, thus causing a significant system downtime and associated costs [8], [9].

The voltage sag sensitivity of an induction motor still exists when the motor is connected through a conventional VFD, in which an uncontrolled diode rectifier is used to power an intermediate dc-link capacitor and six IGBT switches are used to control the voltage and frequency supplied to the motor. The reported sensitivity threshold levels to grid voltage sag for a conventional VFD vary from 50%–60% to 80%–90% of rated voltage, with duration sensitivities of less than five to six cycles [8], [10]. Field records of voltage sags and subsequent VFD shutdowns indicate voltage sags with duration of 12 cycles or more and having a voltage magnitude below 80% of rated voltage will shutdown a VFD [11]. Even if the motor is completely unloaded, the VFD still remains very sensitive to voltage sags [10]. For ride-through capability improvement, VFD manufacturers responded with new mitigation techniques. One of these is to try to maintain the intermediate dc-link voltage from reaching the low-voltage state that causes a shutdown by the use of the kinetic energy from the motor load [12]. By modifying and controlling the switching algorithm of the inverter and taking into account some inertia in the motor and the load, power can be fed back to the dc bus during the supply voltage dip. With this feature, the VFD can continue to work without stopping and resume normal operation after the grid voltage sag. However, a comparison test of five VFDs from five different manufacturers

Manuscript received June 5, 2015; revised October 20, 2015; accepted November 29, 2015. Date of publication December 17, 2015; date of current version May 20, 2016. This work was supported by the Natural Sciences and Engineering Research Council of Canada (NSERC). Recommended for publication by Associate Editor Andrzej M. Trzynadlowski.

S. Leng is with the Petroleum Institute, 2533 Abu Dhabi, UAE (e-mail: sleng@pi.ac.ae).

A. R. N. M. R. Haque and J. Salmon are with the University of Alberta, Edmonton, T6G 2V6 AB, Canada (e-mail: arnmreaz@ualberta.ca; john.salmon@ualberta.ca).

N. Perera was with the University of Alberta, Edmonton, T6G 2V6 AB, Canada. He is now with the Department of Electrical and Electronic Engineering, University of Peradeniya, 20400 Peradeniya, Sri Lanka (e-mail: srilak@ualberta.ca).

A. M. Knight is with the University of Calgary, Calgary, T2N 1N4 AB, Canada (e-mail: aknigh@ucalgary.ca).

Color versions of one or more of the figures in this paper are available online at http://ieeexplore.ieee.org.

Digital Object Identifier 10.1109/TPEL.2015.2508422

demonstrated that such ride-through capability of VFDs were not the same [13]. Moreover, it has been shown in [13] that even the best VFD under test could not cope with symmetrical voltage sag at 80% voltage with either 60 or 300 cycles of duration. A voltage sag compensator described in [14]–[17], is used for critical loads. The proposed compensator consists of a three-phase voltage source inverter (VSI) and a coupling transformer for serial connection. When the grid is at its nominal level, the compensator is bypassed. During grid voltage sags, the compensator injects the required compensation voltage through the coupling transformer. However, long detection time (typically within 4 ms) and large inrush currents can trigger the overcurrent protection, which leads to compensation failure [17].

One of the power converters that have gained importance in current years is the back-to-back (BTB) converter, which is constituted by two voltage source converters (VSCs) and a common energy storage element, a dc capacitor. It is used in renewable energy systems (based on wind turbines (WT) [18], [19] or distributed generation (DG) systems [20]–[22]), HVDC systems [23]–[26], and motor drive systems [27], [28]. The performance of the BTB converter can also be affected by the variable conditions of the electrical grid system; voltage unbalance and voltage sags are the main source of voltage disturbances in this type of system [29]. The unbalanced grid voltage and voltage sag conditions cause instability in the dc-link voltage, which, in turn, can cause loss in power transfer or generate overcurrents that damage the power devices and active protection [30]. For DG systems, the entire transmission and distribution system can lead to instability when electrical disturbances appear in the grid [21]. In HVDC systems, high-power electronic converters are desired to operate with relatively low switching frequencies (maximum 9–15 times the line frequency and even lower for multilevel converters). The low switching frequency operation of VSC systems imposes control limitations in the case of power system faults and disturbances when they may be needed the most. In presently installed operating systems, the ride-through capability is obtained either by using passive element design [24] or a change in the control mode [24] or using overrated power electronics devices [18]. Most of the control solutions to mitigate voltage unbalance is based on either the rotating-frame solution [24], [29], [30] or the stationary-frame solution [31]–[33]. The major disadvantage of the rotating-frame solution is its complexity, which causes a high computational burden [33]. Again, low-pass, band-stop, and notch filters are used in control algorithms to detect a voltage sag in the system; but their response can be too slow [19]. For the BTB converter used in a motor drive application [27], [28], appropriate filters (either *L* or *LCL*) have to be inserted between the grid and the front-end rectifier to reduce the current harmonics around the switching frequency: note that filter inductors are also commonly used at the drive output terminals. The use of these filters increases the system overall size and cost and has been identified as a major barrier to increased power density [34]. BTB converters can also suffer from low efficiencies if the rated motor voltage is lower than the grid input voltage: the input voltage is boosted by the input rectifier; hence, a large voltage step down is then required by the output inverter [35]. Moreover, with a standard BTB converter (12 switches), the motor line voltage waveform has three stepped voltage levels equal to the size of the dc-link voltage. This introduces high *dv*/*dt* stresses on the output cables and on the insulation of motor windings and its bearings [36]. If these voltage levels exceed the machine's insulation corona inception voltage, motor winding insulation life will be shortened.

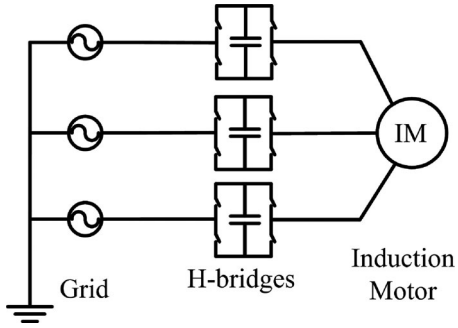

Fig. 1. Three-phase floating capacitor H-bridge converter motor control system.

This study examines a power electronics system in which the voltage sag tolerance of induction motor drive can be greatly improved [37], as shown in Fig. 1.

This proposed three-phase floating H-bridge system employs 12 switches, similar to the BTB converter. It should be noted that the proposed system cannot change the frequency of the voltage supplied to induction motor such as in a VFD. However, the proposed solution is mainly intended to be used in applications where frequency control is not required, e.g., in many applications when using loads such as fans, pumps, and compressors. The system is deemed desirable primarily because of the absence of input and output ac filter inductors, a much lower dc-link operating voltage (producing lower semiconductor device electrical stress, hence the cooling requirements for the power electronics can be made smaller and more cost effective). The overall system operating efficiency can be increased as a result with a higher power density. Moreover, the proposed system can supply five-level motor line pulsewidth-modulated (PWM) waveforms to the induction motor. This voltage compares with the three-level one in a BTB system with much larger voltage steps (see Fig. 2). In steady state, the PWM voltage steps are less than half that experienced in the BTB converter and the motor-induced average volt-secs (closely linked to iron losses in the motor) is much lower. The motor voltage PWM frequencies are four times the device switching frequency as compared to double for the BTB; hence, the motor current ripple is much lower with an associated lowering of the motor high-frequency Cu losses. The H-bridge output PWM voltage waveforms can be said to be much more friendly for the motor cable connections and for the motor winding insulation.

Finally, although the BTB converter can inject reactive power to the grid, this additional functionality requires grid supply reactors, which is often an *LCL* filter, and increases the size and cost of the drive: ac reactors are also routinely added to the output of the drive to minimize the effects of the high-frequency, large-magnitude, PWM voltages at the output terminals. On the contrary, the proposed system inherently generates VARs to the

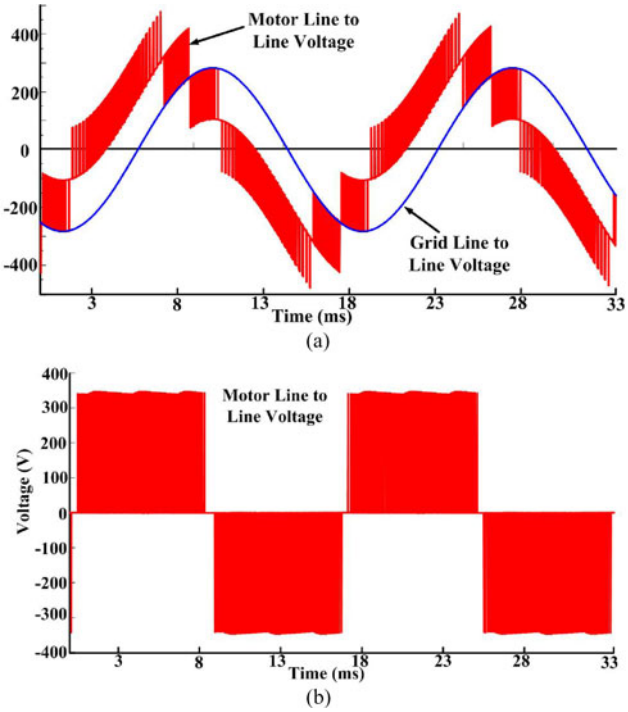

Fig. 2. Motor: (a) line voltage component due to the H-bridges and (b) line voltage component due to BTB converters.

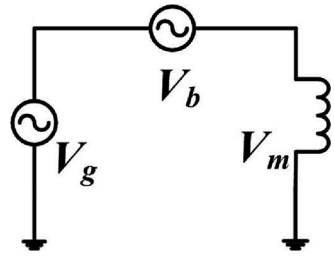

Fig. 3. Simplified per-phase equivalent circuit for the floating capacitor H-bridge inverter motor drive system.

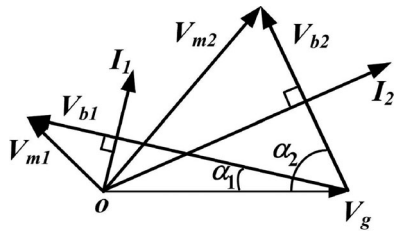

Fig. 4. Phasor diagram for floating capacitor H-bridge converter motor control system.

grid without requiring a grid supply reactor, which has the effect of reducing the system overall cost. It is well known that induction motors naturally operate with a lagging power factor, and they are the main contributor to the total reactive power demand of any given power system [38]. Despite many attempts to compensate the reactive power of a grid-connected induction machine, the majority of these technologies cannot provide voltage-sag ride-through capability. Examples are: 1) reactive current injection such as capacitor banks or STATCOMs [39], [40]; 2) parallel auxiliary windings in the machine [41]; 3) rotating converters [42]; and 4) open-winding induction machine with one terminal connected to a power electronic converter [43]. The proposed system is compatible with standard power distribution practices and, therefore, has the potential in retrofit applications. In summary, the three-phase floating H-bridge system has many desirable features when used to connect an induction motor to the utility grid, including the following:

1) a five-level PWM motor line voltage with a PWM frequency four times the switching frequency and reduced voltage step sizes, resulting in lower higher frequency PWM-induced iron losses and Cu losses;
2) has a relatively higher operating efficiency and lower cooling requirements for the power electronics and the machine;
3) incurs lower system losses, which can lower energy bills, improve the power rating of the machine, reduce its operating temperature, and prolong its operating lifetime;
4) generates VARs and, hence, improves the overall system power factor rather than lowering it;
5) maintains motor voltage at its rated level during grid voltage disturbances (sags and swells);
6) improves motor operating efficiencies under a mismatch condition between grid voltage and rated motor voltage;
7) optimizes the machine power conversion efficiency as the load changes and, hence, saves energy cost, lowers the machine operating temperature, and extends the lifetime of the machine;
8) has a controllable motor voltage, which allows the power electronics to function as a motor soft start.

Some of the aforementioned topics are out of the scope of this paper, which has the focus on the system response to grid voltage sags. A significant voltage sag tolerance has been demonstrated by the proposed three-phase H-bridge system [37]. This paper describes the system control required to compensate for voltage sag ride-through conditions and also defines the relationships between the grid voltage sag compensation limits and the machine load and its operating power factor. The resulting grid reactive power generation characteristics are also presented as a function of the motor load and power factor. Analysis is presented to accurately predict these relationships.

II. Operating Principle and Motor Voltage Control

The steady-state operating principle of the proposed system can be illustrated using a single-phase circuit (see Fig. 3) and a voltage vector diagram representing one phase of the motor with injected bridge voltage (see Fig. 4).

A single-phase floating capacitor H-bridge inverter is modeled as a variable-voltage source, which injects a fundamental voltage V_b in series with the utility grid voltage V_g and the induction machine phase voltage V_m. By controlling the phase and magnitude of the injected voltage V_b: (a) the motor voltage can be reduced lower than the grid voltage, such as required for soft starting the motor (V_{m1} in Fig. 4); (b) increase the motor voltage above the grid voltage, such as maintaining the motor

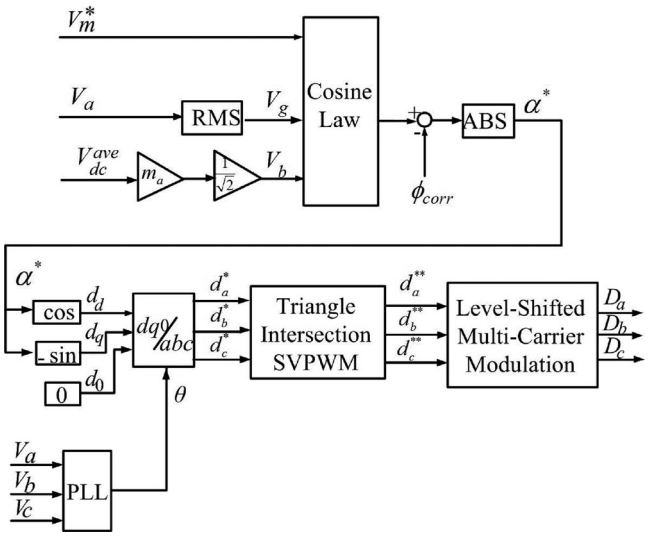

Fig. 5. Control block diagram.

voltage at its rated value when the grid voltage is reduced (V_{m2} in Fig. 4).

Motor voltage control is achieved by changing the angle α (the angle between the grid voltage vector V_g and the bridge voltage vector V_b, as shown in Fig. 4). In general, the higher the α, the higher is the motor voltage and vice versa. However, if the grid voltage magnitude V_g and phase is known together with the bridge dc voltage $V_{\rm dc}$, then the angle α can be set by the controller, using the vector relationships shown in Fig. 4, to supply the motor at a specific desired operating voltage V_m^* such that

$$\cos\alpha^* = \frac{(V_b)^2 + (V_g)^2 - (V_m^*)^2}{2V_bV_g} \tag{1}$$

V_g represents the measured rms value of the grid voltage. Note that V_m^* represents the desired signal for the induction motor terminal voltage. Under soft start mode, V_m^* can be gradually ramped up in a way so that the motor current can be limited. After soft starting, V_m^* can then be made to supply the motor at its rated voltage for optimal motor operation. V_b is the fundamental component of the voltage injected by the H-bridge, assuming sinusoidal PWM control

$$|V_b| = \frac{V_{\rm dc}^{\rm ave} m_a}{\sqrt{2}}. \tag{2}$$

The H-bridge and induction motor system works by defining the desired motor voltage V_m^* (see Fig. 5). For a measured grid voltage V_g, and $V_{\rm dc}$, the voltage V_m^* can be delivered to the motor; but $V_{\rm dc}$ may be in transition due to the bridge current voltage not being at 90° to its fundamental output voltage V_b. However, a specific value for α exists that will result in $V_{\rm dc}$ reaching its steady-state value and producing the desired value for V_m^*. When steady state is achieved, the bridge capacitors stop charging/discharging due to the motor current being at 90° to the bridge voltage V_b.

Note that m_a represents the modulation index of the H-bridge (see Fig. 5). The PWM modulation method used in this paper uses zero-sequence signal injection to determine the modulation index. The theoretical upper limit for m_a using zero-sequence injection is 1.15. In reality, m_a is fixed and set to be slightly lower (1.12 in this study) and kept fixed to minimize the operating voltage of the bridge capacitors. The single-phase currents flowing through the H-bridges naturally produce a low-frequency ripple (120 Hz) in the bridge capacitor voltages. Measuring and taking the average of the three dc capacitor voltages lower the ripple in the dc voltage feedback signal $V_{\rm dc}^{\rm ave}$. The control block diagram used for the three-phase H-bridge controller is shown in Fig. 5.

In Fig. 5, the reference signal for α^* is derived from (1). A phase correction signal $\phi_{\rm corr}$ was set at 5° in the experimental system to take into account various signal phase delays, such as PWM signal generation delays, but mainly the 5 kHz clocking frequency delay of the dSPACE controller (=200 μS or 4.3°). A phase-locked loop (PLL) is used to track the grid voltage angle (θ), which is then used to perform the inverse Park's transformation converting the *dq*0 frame modulation signal d_d, d_q, d_0 into the *abc* frame modulation waves d_a^*, d_b^*, d_c^*. These three phase signals are then converted into signals suitable for SVPWM [44]–[46]: the modified modulation signals d_a^{**}, d_b^{**}, d_c^{**}, which can include the zero-sequence signal. Finally, comparison of the modified modulation signals d_a^{**}, d_b^{**}, and d_c^{**} with level-shifted multicarrier control signals yields the gating signals D_a, D_b, and D_c for the H-bridges to generate five-level PWM line voltage waveforms [47].

III. Grid Voltage Sag Tolerance

The series voltage injected by the H-bridge can be used to compensate for grid voltage sag and thus decouple the motor from the effects of the voltage sag. There is a limit to which the power electronics can compensate for voltage sag, defined as the critical condition. The nature of the voltage sag compensation is described in this section. The voltage sag limit ($S_{\rm min}$) and the grid minimum voltage ($V_g^{\rm min}$) for this compensation are defined in relation to the motor-rated operating voltage $V_m^{\rm rated}$, the motor fundamental power factor (FPF$_m$), and the nominal grid voltage $V_g^{\rm rated}$. The behavior of the system under voltage sag is illustrated using the phasors in Fig. 6.

To illustrate the voltage sag ride-through capability of the system, two important assumptions are made:

1) the load condition on the induction motor remains unchanged;
2) the induction motor terminal voltage is kept at its rated value by the H-bridge controller.

Under these assumptions, if the grid voltage is reduced, from V_{g1} to V_{g2} [see Fig. 6(a)], the angle α increases from α_1 to a_2. As the motor operates at its rated voltage under constant load, the motor fundamental current angle ϕ_m remains the same. As a result, the trajectories of motor voltage V_m and motor current *I* travel along the loci as arcs centered at point *O*. As the severity of the sag increases and V_g is reduced, the angle α increases until a critical condition is reached, where $\alpha = 90°$, as illustrated in Fig. 6(b). Under the critical condition shown in Fig. 6(b), the motor current *I* and grid voltage V_g are in phase with each

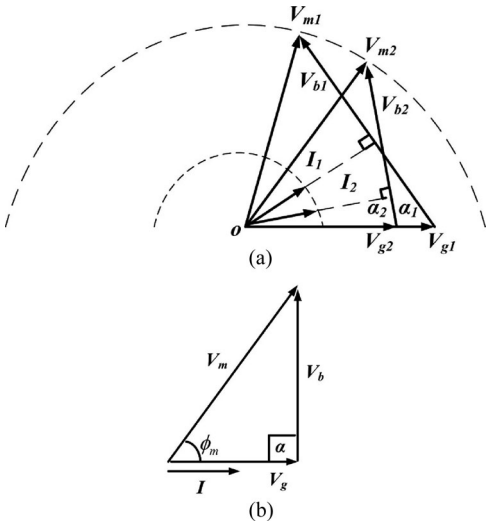

Fig. 6. Phasor diagram illustrating the system response to grid voltage sag: (a) during voltage sag: V_{g1} goes to V_{g2} and (b) critical condition.

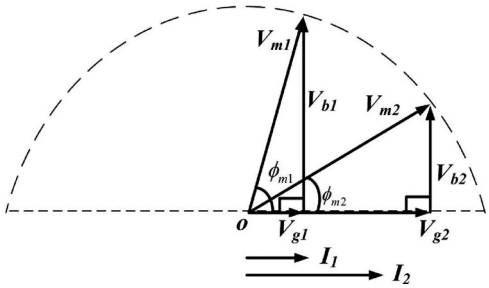

Fig. 7. Effect of the motor power factor angle ϕ_m on the critical condition for the permissible maximum voltage sag compensation.

other and the system is operates with unity power factor at the grid interface. Any further reduction in the grid voltage V_g beyond this critical condition results in collapsing of the H-bridge dc capacitor voltages and, consequently, collapsing of the induction motor terminal voltage V_m. Therefore, the severity of voltage sag that the proposed H-bridge system can ride through is determined by the magnitude of the motor power factor angle f_m under the critical condition (see Fig. 7).

For an induction motor with a constant motor terminal voltage, different load conditions will result in a different FPF_m angle ϕ_m. Considering Fig. 7, it can be seen that the shape of the right-angle triangle obviously changes with ϕ_m. Therefore, the magnitude of V_g under the critical condition, and thus the voltage sag ride-through capability of the system, will be a function of ϕ_m. Under a no-load condition, since the magnetizing current forms a major component of the motor current, the motor power factor may be as low as 0.1–0.3 [48], which results in a high value for $\phi_m (= 75^\circ$ to $85^\circ)$ (see Fig. 7). Therefore, a small grid voltage V_{g1} can be boosted with the help of a bridge voltage V_{b1} to maintain the motor at the rated terminal voltage V_{m1}. This means that if an induction motor is operating under very light load, the grid voltage sag can go as low as 10%–30% of the rated motor voltage while still maintaining the induction motor at its rated voltage. However, under normal conditions (80%–100% of the full load), the FPF_m increases to typically 0.8–0.9 [48]. This means that the grid voltage sag that may be endured may lie in the 80%–90% range of the rated motor voltage.

Expressing these conditions mathematically, the voltage sag ride-through capability depends on the FPF_m and can be expressed as

$$V_g^{\min} = V_m^{\text{rated}} \cos\emptyset_m = V_m^{\text{rated}} \text{FPF}_{\text{m}} \tag{3}$$

where $V_g^{\min}$ represents the minimum grid voltage that the proposed H-bridge induction motor drive system can cope with. V_m^{rated} represents the rated induction motor voltage, which is assumed to be kept constant and can be obtained from the nameplate of the motor. FPF_m represents the FPF_m, which is determined by the motor load condition. This relationship is confirmed in this study using experimental results.

The proposed three-phase floating H-bridge system is compatible with standard power distribution practices and has great potential in retrofit applications. An interesting point to note is that common practice often results in using the induction motors that are often oversized due to an overestimation of the mechanical power required by the load [49]. In both the industrial and tertiary sectors in the European Union, the average induction motor power factor is low at $\text{FPF}_m = 0.57$ [50]. Therefore, if retrofitted with the proposed three-phase floating H-bridge system, a symmetrical grid voltage sag of 60% indefinitely relative to the rated induction motor terminal voltage will not trip out the motor. Depending on the grid voltage applied, the severity of the voltage sag (in percentage) that the proposed H-bridge system can cope with is calculated as

$$s_{\min} = \frac{V_m^{\text{rated}} \text{FPF}_m}{V_g^{\text{rated}}} \times 100\% \tag{4}$$

where $s_{\min}$ represents the severity of voltage sag relative to nominal grid voltage and V_g^{rated} represents the rated grid voltage. As an example, if the motor is operated at a rated voltage of 230 V with a power factor of 0.82 (= full load), then operating from a grid voltage of 208 V gives a value for $s_{\min}$ at 0.91: if the motor power factor is 0.3 (light load), then $s_{\min}$ becomes 0.33.

IV. Motor Fundamental Current Angle Estimation

Determining the voltage sag ride-through capability of the three-phase floating H-bridge motor control system and predicting a value for the voltage sag limit ($S_{\min}$) depend upon knowing the exact value for motor fundamental power factor (FPF_m). FPF_m varies with the motor load conditions, and direct measurement of this quantity is not practically feasible due to the voltage PWM waveforms experienced at the motor terminals and noise interference. One solution is to apply a low-pass filter on feedback signals; however, this may experience noise problems, attenuation, and signal delays and introduce phase shifts in the motor voltage being monitored. These effects may have a negative impact on the accuracy of the power factor measurement. Alternatively, the motor power factor angle ϕ_m during

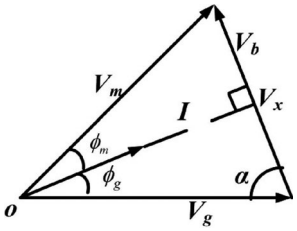

Fig. 8. System vector diagram under nominal steady-state operating conditions to predict the FPF_m angle.

nominal grid steady-state operating conditions can be estimated if the power factor angle ϕ_g at the grid can be measured reliably. The controller (see Fig. 5) is designed to monitor the utility grid parameters accurately using a PLL, and the grid voltage and current can be monitored reliably and are natural signals to use in the controller. Consider Fig. 8 and assume that the magnitude of the grid phase voltage V_g can be measured.

The average dc capacitor voltage of the three H-bridges in the proposed system can be measured as

$$V_{\text{dc}}^{\text{ave}} = \frac{V_{\text{dc}}^a + V_{\text{dc}}^b + V_{\text{dc}}^c}{3}. \tag{5}$$

The modulation index m_a of the H-bridge is kept fixed at its maximum ($m_a = 1.12$ was used in this study), and the fundamental component of the bridge voltage injected per phase V_b is calculated as in (2). Using a PLL to track the grid voltage angle θ (see Fig. 5), measurement of the three-phase grid currents using Park's transformation can then be used to obtain the grid current angle $\phi_g = a\tan(I_q/I_d)$.

Assuming that the bridge losses are negligible, V_b is approximately at 90° degrees relative to *I* (known error angles can be used to correct for any differences)

$$\alpha = 90^\circ - \phi_g. \tag{6}$$

Applying the law of cosines and using phase quantities, the motor terminal voltage can be obtained as

$$V_m = \sqrt{V_g^2 + V_b^2 - 2V_gV_b\cos\alpha}. \tag{7}$$

Now, it is possible to construct an imaginary voltage vector V_X aligned with *I* (see Fig. 8). The length of the imaginary voltage vector V_x is

$$V_x = V_g\cos\phi_g. \tag{8}$$

Finally, given that V_b is approximately at 90° relative to V_x, motor fundamental power factor angle ϕ_m can be estimated as

$$\emptyset_m = \cos^{-1}\frac{V_x}{V_m} = \cos^{-1}\left(\frac{V_g}{V_m}\cos\phi_g\right). \tag{9}$$

This relationship is verified in this study with experimental results. Assuming a measured grid phase angle of 30°, $V_g = 208$ V and $V_m = 230$ V (using line voltage equivalents), then $\phi_m = 38.4$; and the maximum, or critical, voltage sag from (4) has $s_{\min} = 0.87$.

V. Reactive Power Generation

Under both nominal system operating conditions and under conditions of grid voltage sag, the system current leads the grid voltage (see Figs. 6–8). This represents VAR generation into the grid, and analysis is presented to predict the VAR generated under nominal and voltage sag conditions.

The voltage injected by the H-bridge (V_b) phase shifts the induction motor terminal voltage (V_m) so that it leads the grid voltage (V_g) (see Fig. 8). As a result, the induction motor current vector (*I*) also leads the grid voltage (V_g), generating VARs instead of consuming. Taking into account the fact that the voltage vector V_X is in phase with *I*, the power factor of the proposed three-phase floating H-bridge system, as seen at the grid terminals, can be expressed as

$$\text{FPF}_g = \cos\emptyset_g = \frac{V_X}{V_g}. \tag{10}$$

In steady state, the grid leading fundamental power factor (FPF_g) can be expressed as

$$\text{FPF}_g = \frac{V_m}{V_g}\text{FPF}_m. \tag{11}$$

Equation (11) implies that the utility FPF_g is proportional to lagging motor FPF_m, as long as the grid voltage (V_g) and motor voltages (V_m) are kept constant. This means that with an increasing motor load, the motor and the utility grid fundamental power factors increase. The relationship in (11) is confirmed in this study with experimental results. In steady state, the proposed system supplies reactive power to the utility grid and, thus, improves the overall system VAR requirement. During grid voltage sags, V_g obviously decreases and the grid fundamental power factor increases from (11). The VARs that are generated into the grid can be calculated as

$$Q = \sqrt{3}V_gI\sin\emptyset_g \tag{12}$$

$$Q = \sqrt{3}I\sqrt{(V_g)^2 - (V_m)^2\,(\text{FPF}_m)^2}. \tag{13}$$

Under constant motor voltage operation, as the motor load increases, both the motor current *I* and FPF_m increase. Equation (13) implies that if the utility grid voltage remains constant and the proposed H-bridge system can maintain the motor terminal voltage at its rated value, then a load increase does not necessarily result in an increase or decrease of the VARs being generated. Equation (13) and the effect of load change are investigated further using experimental results.

However, consider the voltage sag: if the motor voltage and its load is assumed constant, the motor current is constant. Let us assume a motor line voltage of 230 V, current of 13.6 A, and FPF_m of 0.82 lagging. Comparing a nominal grid voltage of 208 V, with a 5% sag condition of 197.6 V, the grid VARs generated change from 1192 to 802 VA, with ϕ_g changing from leading by 24.9° to leading by 17.4°, as expected from Fig. 6. These trends are investigated further with experimental results.

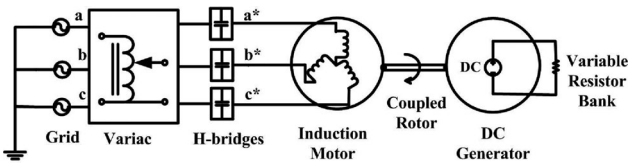

Fig. 9. Test platform schematic.

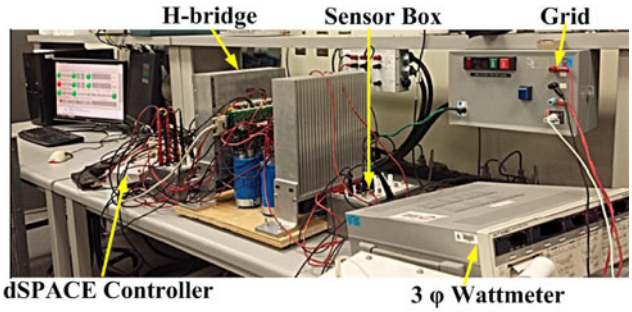

(a)

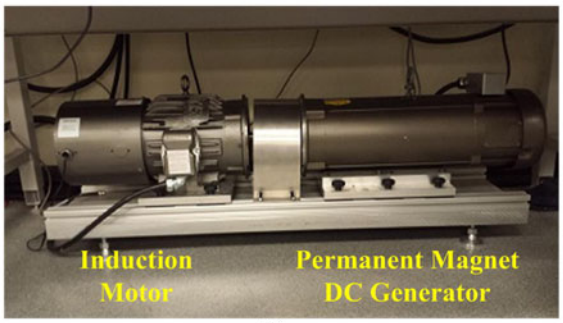

(b)

Fig. 10. Experimental test facility: (a) H-bridge system with dSPACE controller and (b) induction motor with PMDC generator.

VI. Experimental Validation

A 230-V 5-hp motor–generator set was used as the test platform. The schematic for the test platform is shown in Fig. 9. A variac is used to step down the 208 V/60 Hz input voltage to the test system to emulate balanced three-phase voltage sag. Three single-phase floating H-bridges are installed between the variac and the induction motor. A permanent-magnet dc (PMDC) generator is mechanically coupled with the induction motor, and a variable resistor bank is connected to the dc generator armature terminals to act as a variable load. Experimental test facility is shown in Fig. 10.

The converters used in the experiment are custom-made IGBT-based power converters. The converters use Semikron (SKiM306GD12E4) IGBT modules. The single-phase floating H-bridges were made up of two separate inverter legs, each with a 4-mF dc capacitor with a voltage rating of 500 V. Through parallel connection, the equivalent capacitance per phase is 8 mF. The induction motor was a general-purpose 5-hp 60-Hz/50-Hz NEMA premium motor. The induction motor was a four-pole inverter duty motor rated at 5 hp, 60 Hz, 230/460 V, 13.6/6.5 A, 1760 r/min (6000 r/min maximum). The motor nominal efficiency is 90.2% and 0.82 PF under full load. The load dc machine was rated at 5 hp 180 V, 21.6 A, 1750 r/min, type 3681P TEFC, and design B, with a nominal efficiency of 84% and is connected to a variable resistor bank that is rated at 250 V with a resistance ranging from 7.81 to 83.3 Ω. The control algorithm is implemented on a dSPACE DS1104 platform, with a sampling frequency of 5 kHz and a switching frequency of 7.5 kHz.

A. Voltage Sag Tolerance

The experimental three-phase floating H-bridge motor control system was proven capable of boosting the motor voltage to its rated value (230 V) when operated from a 208 V grid and maintained the rated motor voltage under voltage sags of various magnitudes (depending on the motor load conditions) (see Fig. 11). Under full-load condition, the motor is operated at a 0.76 power factor lag, with a rated voltage sustained at a voltage sag of 176.5 V [see Fig. 11(a)]. When the motor is under half load, it operates at a 0.58 power factor lag and with a grid voltage dips down to 137.5 V [see Fig. 11(b)]. Under no-load condition, motor operates at a 0.15 power factor lag and the system tolerates maximum voltage sag down to 32 V [see Fig. 11(c)].

In brief, the experimental results in Fig. 11 established the following:

1) induction motor terminal line voltage can be maintained at its rated value (230 V) for significant periods of time (no less than hundreds of cycles) during voltage sags under various load conditions;
2) the magnitude of the motor current stays the same during voltage sag;
3) the lower the motor load, the deeper the voltage sag that can be tolerated while maintaining rated motor voltage.

Another set of experimental results are presented to demonstrate the voltage sag critical condition. Experimental results for three different load conditions were taken under different grid voltages (see Figs. 12–14): full load ($I = 13.6$ A, $\text{FPF}_m = 0.755$); half load ($I = 10.3$ A, $\text{FPF}_m = 0.581$); and no load ($I = 7$A, $\text{FPF}_m = 0.146$). In these results, motor terminal voltage is boosted to its rated value (230 V) by the three-phase H-bridge. For each load setting, the motor power factor remains the same for each set of results as the motor voltage is unchanged. Figs. 12–14 are actually another way of representing the phasor diagram shown in Fig. 6(a). In all situations, the critical condition is reached when grid fundamental power factor becomes unity [see Figs. 12(c), 13(c), and 14(c)].

To validate the concept of voltage sag tolerance as identified in (3), the motor power factor angle under various load conditions were recorded using the estimation technique described in Section IV. A FLUKE 39 power meter was used to monitor the induction motor terminal voltage. A variac was used to simulate symmetrical voltage sags of different magnitudes. Close attention was paid to record the deepest voltage sag without collapsing of the induction motor terminal voltage ($V_{m,\text{line}} = 230$ V). The experimental results of maximum voltage sag agreed very well with theoretical predicted values (see Fig. 15).

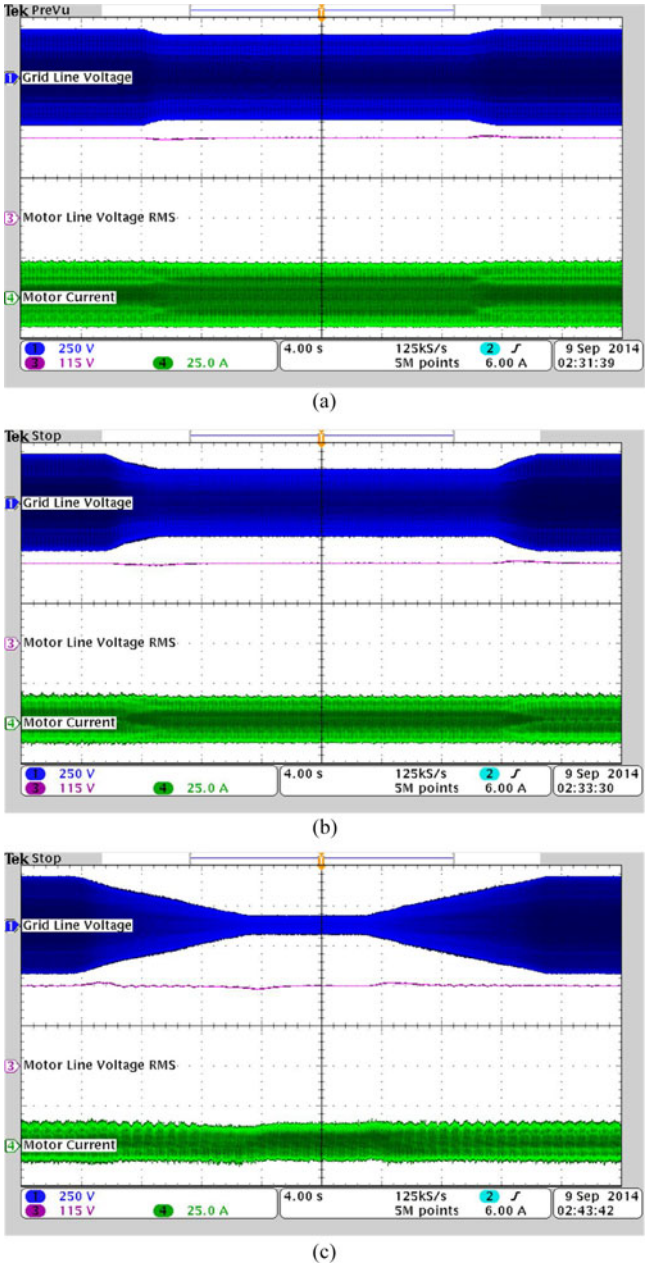

Fig. 11. Voltage sag ride-through performance: (a) full-load, voltage sag 85% of rated grid voltage; (b) half-load, voltage sag 66% of rated grid voltage; (c) no load, voltage sag 16% of rated grid voltage

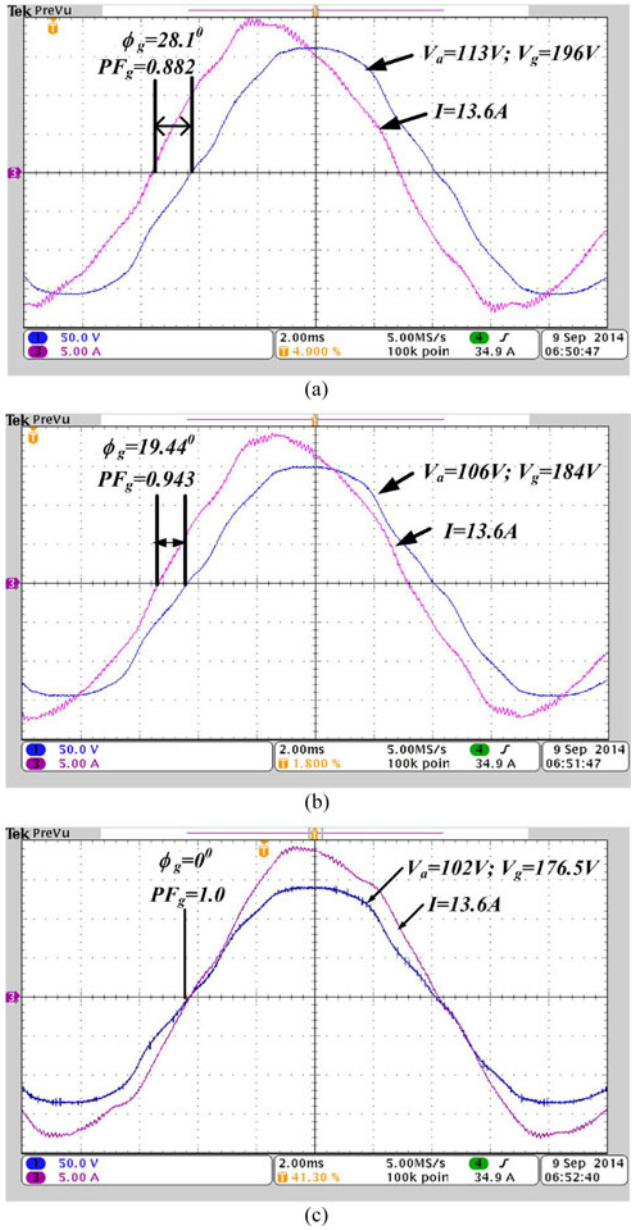

Fig. 12. Reactive power generation of the proposed H-bridge induction motor drive system under the full-load condition ($I = 13.6$ A, FPF$_m = 0.755$): (a) $V_g = 196$ V, (b) $V_g = 184$ V, and (c) $V_g = 176.5$ V.

To demonstrate the maximum voltage sag tolerance, $s_{\min}$ is plotted in Fig. 16. Under maximum load conditions, the proposed power electronics system can tolerate a $s_{\min}$ of 82%: voltage sag up to 18% of the rated grid voltage for continuous periods.

B. Reactive Power Generation

Reactive power generation capability of the proposed H-bridge system under constant grid voltage ($V_g = 208$ V) and constant motor terminal voltage ($V_m = 230$ V) but under variable motor load conditions (from no load to full load) is shown in Fig. 19. Under fixed grid voltage and constant motor voltage, the grid reactive power generation depends on the FPF$_m$ (13). Figs. 17 and 18 compare the theoretical and experimental predictions of the grid fundamental power factor angle and the motor fundamental current angle. Experimentally, the grid and FPF$_m$ angles were measured using a FLUKE 39 power meter. Simulations were also carried using MATLAB Simulink simulations. Experimental and theoretical values for the motor fundamental current angle (ϕ_m) (see Fig. 17) were in good agreement: the difference experienced with the simulation results were could be caused by parameter variations in the motor model used.

The experimental fundamental grid angle (ϕ_g) is plotted as a function of the motor load in Fig. 18 and compared with

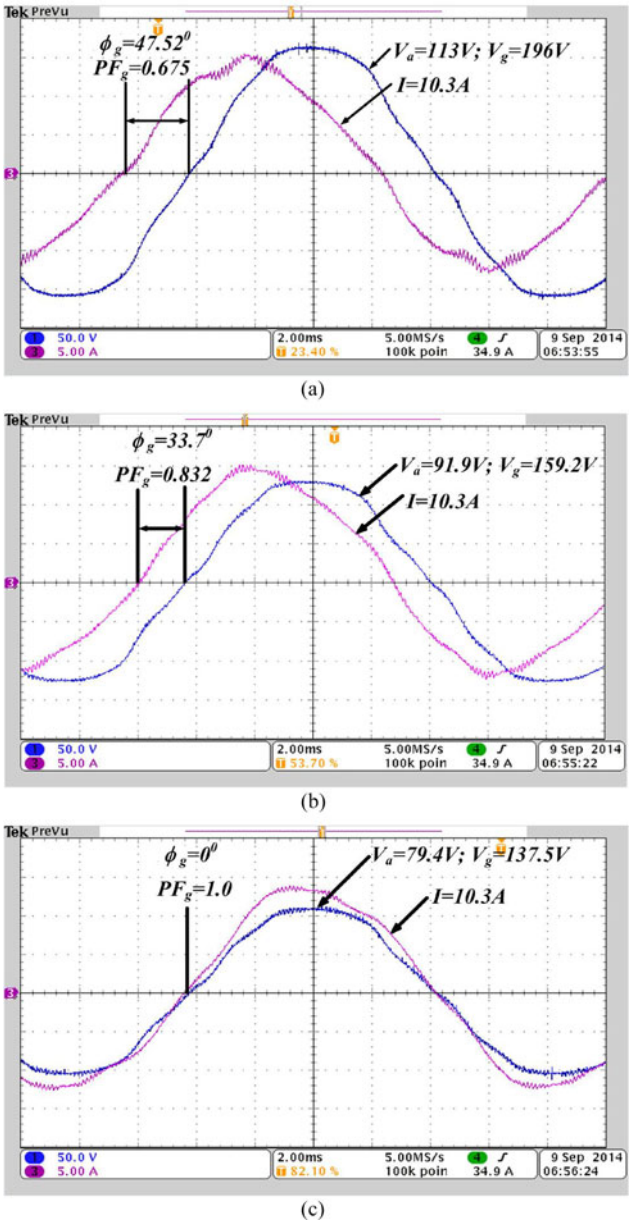

Fig. 13. Reactive power generation of the proposed H-bridge induction motor drive system under the half-load condition ($I = 10.3$ A, FPF$_m = 0.581$): (a) $V_g = 196$ V, (b) $V_g = 159.2$ V, and (c) $V_g = 137.5$ V.

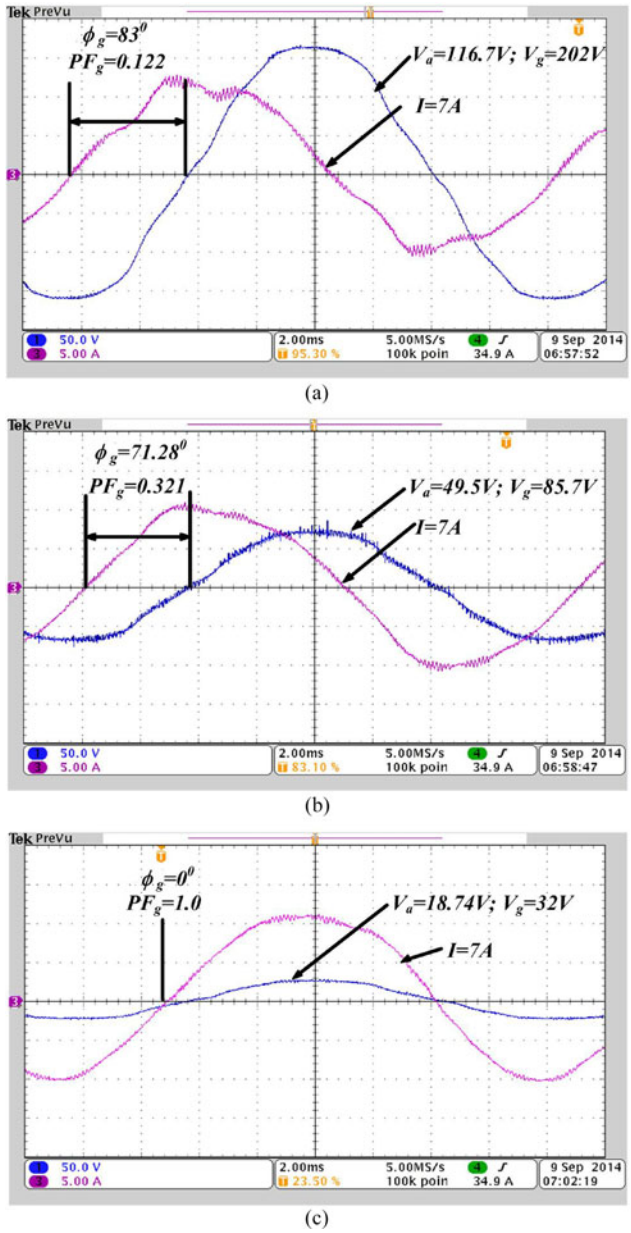

Fig. 14. Reactive power generation of the proposed H-bridge induction motor drive system under no load condition ($I = 7$ A, FPF$_m = 0.146$): (a) $V_g = 202$ V, (b) $V_g = 85.7$ V, and (c) $V_g = 32$ V.

theoretical predictions using (11): the motor is operated at rated 230 V and the grid at 208 V. In steady state, as the motor load is increased, ϕ_g goes down (V_m and V_g are constant, but ϕ_m decreases with an increasing load), thus resulting in an increasing fundamental power factor at the point of coupling (PCC).

Good agreement is obtained between theoretical predictions using (13) and experimentally measured values, as can be seen in Fig. 19. The slight deviation between predictions and measured results could be caused by the impedance of the variac used.

The reactive power delivered to the grid remains relatively flat despite the large variations in the motor load. This means, approximately, the operation of the proposed three-phase

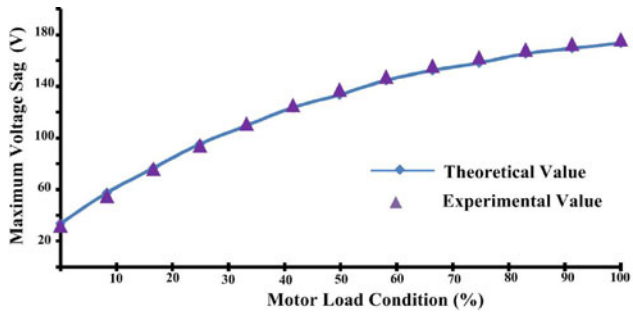

Fig. 15. Comparison between theoretical and experimental values of maximum voltage sag while maintaining the rated motor voltage.

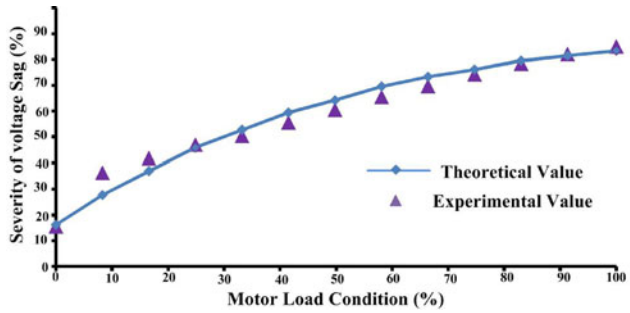

Fig. 16. Severity of voltage sag as a function of load condition.

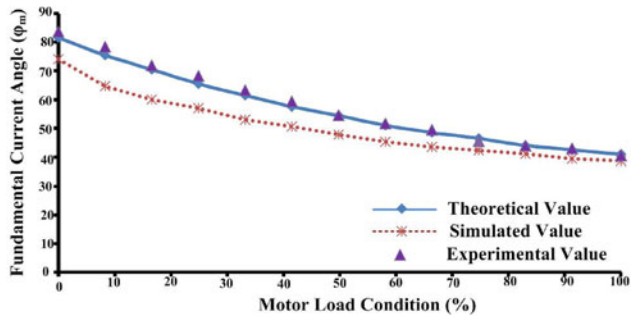

Fig. 17. Comparison of the motor fundamental current angle (ϕ_m) lag as a function of the motor load condition [see (9)].

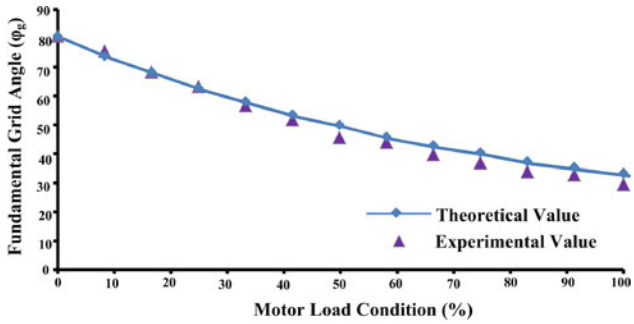

Fig. 18. Comparison of fundamental grid angle (ϕ_g) as a function of the motor load condition.

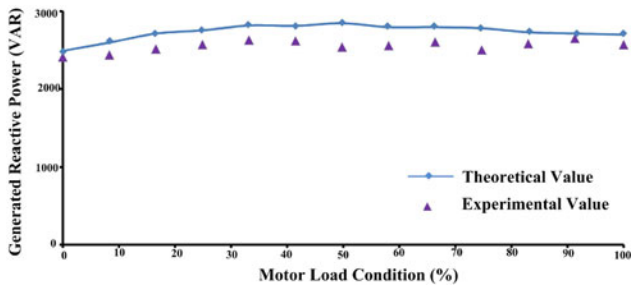

Fig. 19. Reactive power generation trend of the proposed H-bridge induction motor drive system.

floating H-bridge and induction motor can be modeled as a constant reactive power generator for the grid.

VII. Conclusion

The voltage sag ride-through capability of a three-phase floating capacitor H-bridge system was presented that was used to control the voltage of an induction machine. A controller was described that changed the angle of the injected voltage by the three-phase H-bridges to control the motor voltage at some constant desired value, such as the motor rated voltage, even during periods of grid voltage sag. The reactive power generation capability of this system was presented as a function of the motor load and the degree of grid voltage sag experienced. The effectiveness of the voltage sag ride-through capability of the proposed system was closely related to the motor power factor angle. Generally, the higher the induction motor load, the lower the tolerance of the system to grid voltage sags. The lowest tolerance happened when the induction motor was fully loaded and when the motor power factor was at its highest. Theory was presented that allowed the largest voltage sag to be predicted, or alternatively the lowest grid voltage, while maintaining the motor at its rated voltage. Unity power factor operation of the proposed H-bridge system is possible, which also corresponds to the critical condition for the maximum voltage boosting of induction motor voltage. Further reduction in grid voltage beyond the critical condition resulted in the collapsing of the H-bridge dc capacitor voltages and, consequently, collapsing of the induction motor terminal voltage. As the motor load increased under constant motor voltage control, the power factor of the proposed H-bridge, as seen at the utility grid, increased with the motor power factor. However, the reactive power generated by the proposed H-bridge system remained relatively flat despite variations in the motor load, which means the proposed system can be modeled as constant reactive power generator for the grid.

Acknowledgment

The authors would like to thank A. Terheide for helping in constructing the power electronics involved and the University of Alberta for providing the facilities.

References

[1] Y. Zhang, J. Zhu, Z. Zhao, W. Xu, and D. G. Dorrell, "An improved direct torque control for three-level inverter-fed induction motor sensorless drive," *IEEE Trans. Power Electron.*, vol. 27, no. 3, pp. 1502–1513, Mar. 2012.

[2] Y. He, Y. Wang, Y. Feng, and Z. Wang, "Parameter identification of an induction machine at standstill using the vector constructing method," *IEEE Trans. Power Electron.*, vol. 27, no. 2, pp. 905–915, Feb. 2012.

[3] S. A. Davari, D. A. Khaburi, F. Wang, and R. M. Kennel, "Using full order and reduced order observers for robust sensorless predictive torque control of induction motors," *IEEE Trans. Power Electron.*, vol. 27, no. 7, pp. 3424–3433, Jul. 2012.

[4] A. de Almeida, P. Bertoldi, and H. Falkner, *Energy Efficiency Improvements in Electric Motors and Drives*. Berlin, Germany: Springer-Verlag, 2000.

[5] S. Hardi, S. Hs, M. Hafizi, Z. Pane, and R. Chan, "Induction motors performance under symmetrical voltage sags and interruption—Test result," in *Proc. IEEE 7th Int. Power Eng. Optim. Conf.*, 2013, pp. 630–635.

[6] J. C. Gomez, M. M. Morcos, C. A. Reineri, and G. N Campetelli, "Behavior of induction motor due to voltage sags and short interruptions," *IEEE Trans. Power Del.*, vol. 17, no. 2, pp. 434–440, Apr. 2002.

[7] E. W. Gunther and H. Mehta, "A survey of distribution system power quality—Preliminary results," *IEEE Trans. Power Del.*, vol. 10, no. 1, pp. 322–329, Jan. 1995.

[8] M. H. J. Bollen, "Understanding power quality problems," *Voltage Sags and Interruptions*, 1st edn, New York, NY: Wiley-IEEE Press, Sep. 1999.

[9] F. Carlson, "Before and during voltage sags: The relationship between the voltages and the tripping level for line-operated machines," *IEEE Ind. Appl. Mag.*, vol. 11, no. 2, pp. 39–46, Mar./Apr. 2005.

[10] S. Z. Djokic, K. Stockman, J. V. Milanovic, J. J. M. Desmet, and R. Belmans, "Sensitivity of AC adjustable speed drives to voltage sags and short interruptions," *IEEE Trans. Power Del.*, vol. 20, no. 1, pp. 494–505, Jan. 2005.

[11] G. H. Sarmiento and E. Estrada, "A voltage sag study in an industry with adjustable speed drives," *IEEE Ind. Appl. Mag.*, vol. 2, no. 1, pp. 16–19, Jan./Feb. 1996.

[12] J. Holtz, W. Lotzkat, and S. Stadtfeld, "Controlled AC drives with ride-through capability at power interruption," *IEEE Trans. Ind. Appl.*, vol. 30, no. 5, pp. 1275–1283, Sep./Oct. 1994.

[13] P. Angers and F. Levesque, "Voltage dip immunity of PWM drives with ride-through capabilities," in *Proc. Int. Conf. Electr. Mach.*, 2010, pp. 1–5.

[14] C.-J. Huang, S.-J. Huang, and F.-S. Pai, "Design of dynamic voltage restorer with disturbance-filtering enhancement," *IEEE Trans. Power Electron.*, vol. 18, no. 5, pp. 1202–1210, Sep. 2003.

[15] D. M. Vilathgamuwa, A. A. D. R. Perera, and S. S. Choi, "Voltage sag compensation with energy optimized dynamic voltage restorer," *IEEE Trans. Power Del.*, vol. 18, no. 3, pp. 928–936, Jul. 2003.

[16] P.-T. Cheng, C.-C. Huang, C.-C. Pan, and S. Bhattacharya, "Design and implementation of a series voltage sag compensator under practical utility conditions," *IEEE Trans. Ind. Appl.*, vol. 39, no. 3, pp. 844–853, May–Jun. 2003.

[17] Y.-H. Chen, C.-Y. Lin, J.-M. Chen, and P.-T. Cheng, "An inrush mitigation technique of load transformers for the series voltage sag compensator," *IEEE Trans. Power Electron.*, vol. 25, no. 8, pp. 2211–2221, Aug. 2010.

[18] R. Ottersten, A. Petersson, and K. Pietiläinen, "Voltage sag response of PWM rectifiers for variable-speed wind turbines," *EPE J.*, vol. 16, no. 1, pp. 6–14, Feb. 2006.

[19] M. Fatu, F. Blaabjerg, and I. Boldea, "Grid to standalone transition motion-sensorless dual-inverter control of PMSG with asymmetrical grid voltage sags and harmonics filtering," *IEEE Trans. Power Electron.*, vol. 29, no. 7, pp. 3463–3472, Jul. 2014.

[20] J. Miret, A. Camacho, M. Castilla, L. G. de Vicuna, and J. Matas, "Control scheme with voltage support capability for distributed generation inverters under voltage sags," *IEEE Trans. Power Electron.*, vol. 28, no. 11, pp. 5252–5262, Nov. 2013.

[21] J. Miret, A. Camacho, M. Castilla, J. L. García de Vicuña, and J. de la Hoz, "Reactive current injection protocol for low-power rating distributed generation sources under voltage sags," in *IET Power Electron.*, vol. 8, no. 6, pp. 879–886, Jun. 2015.

[22] P. Khamphakdi, K. Sekiguchi, M. Hagiwara, and H. Akagi, "A transformerless back-to-back (BTB) system using modular multilevel cascade converters for power distribution systems," *IEEE Trans. Power Electron.*, vol. 30, no. 4, pp. 1866–1875, Apr. 2015.

[23] A. Petersson and A. Edris, "Dynamic performance of the eagle pass back-to-back HVDC light tie," in *Proc. 7th Int. Conf. AC–DC Power Trans. 2001 (Conf. Publ. No. 485)*, 28–30 Nov., pp. 220–225.

[24] B. Parkhideh and S. Bhattacharya, "Vector-controlled voltage-source-converter-based transmission under grid disturbances," *IEEE Trans. Power Electron.*, vol. 28, no. 2, pp. 661–672, Feb. 2013.

[25] T. H. Nguyen, D.-C. Lee, and C.-K. Kim, "A series-connected topology of a diode rectifier and a voltage-source converter for an HVDC transmission system," *IEEE Trans. Power Electron.*, vol. 29, no. 4, pp. 1579–1584, Apr. 2014.

[26] S. Li, X. Wang, Z. Yao, T. Li, and Z. Peng, "Circulating current suppressing strategy for MMC-HVDC based on nonideal proportional resonant controllers under unbalanced grid conditions," *IEEE Trans. Power Electron.*, vol. 30, no. 1, pp. 387–397, Jan. 2015.

[27] S. M. M. Gazafrudi, A. T. Langerudy, E. F. Fuchs, and K. al-Haddad, "Power quality issues in railway electrification: A comprehensive perspective," *IEEE Trans. Ind. Electron.*, vol. 62, no. 5, pp. 3081–3090, May 2015.

[28] J. Lemmens, P. Vanassche, and J. Driesen, "Optimal control of traction motor drives under electrothermal constraints," *IEEE J. Emerg. Sel. Topics Power Electron.*, vol. 2, no. 2, pp. 249–263, Jun. 2014.

[29] R. Sierra, V. Cardenas, J. Alcala, and N. Visairo, "Single-phase analysis of BTB converter under unbalanced voltage conditions," in *Proc. 2011 8th Int. Conf. Electr. Eng. Comput. Sci. Autom. Control*, Oct. 26–28, pp. 1–6.

[30] R. Sierra, J. Alcala, V. Cardenas, J. Perez-Ramirez, and A. Rivera, "Evaluating the performance of the BTB converter under unbalanced voltage sags," in *Proc. 2012 9th Int. Conf. Electr. Eng. Comput. Sci. Autom. Control*, Sep. 26–28, pp. 1–6.

[31] M. Castilla, J. Miret, A. Camacho, L. G. de Vicuna, and J. Matas, "Modeling and design of voltage support control schemes for three-phase inverters operating under unbalanced grid conditions," *IEEE Trans. Power Electron.*, vol. 29, no. 11, pp. 6139–6150, Nov. 2014.

[32] X. Guo, X. Zhang, B. Wang, W. Wu, and J. M. Guerrero, "Asymmetrical grid fault ride-through strategy of three-phase grid-connected inverter considering network impedance impact in low-voltage grid," *IEEE Trans. Power Electron.*, vol. 29, no. 3, pp. 1064–1068, Mar. 2014.

[33] X. Guo, W. Liu, X. Zhang, X. Sun, Z. Lu, and J. M. Guerrero, "Flexible control strategy for grid-connected inverter under unbalanced grid faults without PLL," *IEEE Trans. Power Electron.*, vol. 30, no. 4, pp. 1773–1778, Apr. 2015.

[34] J. W. Kolar, U. Drofenik, J. Biela, M. L. Heldwein, H. Ertl, T. Friedli, and S. D. Round, "PWM converter power density barriers," in *Power Convers. Conf.*, Nagoya, Japan, Apr. 2–5, 2007, pp. 9–29.

[35] R. Cuzner, D. Drews, and G. Venkataramanan, "Power density and efficiency comparisons of system-compatible drive topologies," *IEEE Trans. Ind. Appl.*, vol. 51, no. 1, pp. 459–469, Jan.–Feb. 2015.

[36] R. J. Kerkman, "Twenty years of PWM AC drives: When secondary issues become primary concerns," in *Proc. 22nd IEEE IECON*, Aug. 5–10, 1996, vol. 1, pp. LVII–LXIII.

[37] S. Leng, R. Haque, N. Perera, J. Salmon, and A. M. Knight, "Soft start and voltage control of grid connected induction motors using floating capacitor H-bridge converters," in *Proc. 2014 IEEE Energy Convers. Congr. Expo.*, Sep. 2014, pp. 1309–1316.

[38] P. Waide and C. U. Brunner, "Energy-efficiency policy opportunities for electric motor-driven systems," *Int. Energy Agency, Paris, France, Work. Paper Energy Efficiency Ser.*, OECD/IEA 201.1, 2011.

[39] R. Spee and A. K. Wallace, "Comparative evaluation of power factor improvement techniques for squirrel cage induction motors," *IEEE Trans. Ind. Appl.*, vol. 28, no. 2, pp. 381–386, Mar./Apr. 1992.

[40] C. Wessels, N. Hoffmann, M. Molinas, and F. Fuchs, "StatCom control at wind farms with fixed speed induction generators under asymmetrical grid faults," *IEEE Trans. Ind. Electron.*, vol. 60, no. 7, pp. 2864–2873, Jul. 2013.

[41] M. C. Muteba, A. A. Jimoh, D. V. Nicolae, and A. S. O. Ogunjuyigbe, "Performance evaluation of a three-phase induction machine with auxiliary winding fed by a leading reactive current," in *Proc. Power Energy Syst. (AfricaPES)*, pp. 8–10, Sep. 2008.

[42] N. Malik, C. Sadarangani, A. Cosic, and M. Lindmark, "Induction machine at unity power factor with rotating power electronic converter," in *Proc. Automat. Motion Power Electron. Electr. Drives*, Jun. 2012, pp. 401–408.

[43] A. M. Knight, J. Salmon, R. Haque, N. Perera, and M. S. Toulabi, "A grid-connected induction machine capable of operation at unity and leading power factor," in *Proc. Energy Convers. Congr. Expo.*, Sep. 2013, pp. 238–245.

[44] S. L. Capitaneanu, B. de Fornel, M. Fadel, J. Faucher, and A. Almeida, "Graphical and algebraic synthesis for PWM methods," *EPE J.*, vol. 11, no. 3, pp. 16–28, Aug. 2001.

[45] F. G. King, "Athree phase transistor class-B inverter with sinewave output and high efficiency," in *Proc. IEE Conf. (Publ. 123)*, 1974, pp. 204–209.

[46] L. J. Garces, "Current control of field oriented AC induction motordrives," *IEEE Industry Applications Society, Tutorial Course 1991, Mircoprocessor Control Motor Drives Power Converters*, pp. 5-1–5-33.

[47] B. Wu, "Cascaded H-Bridge Multilevel Inverters", *High-Power Converters and AC Drives*. Hoboken, NJ: Wiley-IEEE Press, Mar. 2006, ch. 7.

[48] A. Ukil, R. Bloch, and A. Andenna, "Estimation of induction motor operating power factor from measured current and manufacturer data," *IEEE Trans. Energy Convers.*, vol. 26, no. 2, pp. 669–706, Jun. 2011.

[49] A. de Almeida, F. E. Ferreira, and P. Fonseca, "Improving the penetration of energy-efficient motors and drives," *ISR-Univ. Coimbra, European Commission, Directorate-G. Trans. Energy, SAVE II Prog.*, Mar. 2000.

[50] A. H. Bonnett, "An overview of how AC induction motor performance has been affected by the October 24, 1997 implementation of the Energy Policy Act of 1992," *IEEE Trans. Ind. Appl.*, vol. 36, no. 1, pp. 242–256, Jan./Feb. 2000.

Siyu Leng (M'14) received the B.Sc. degree from Tongji University, Shanghai, China, in 2006, and the Ph.D. degree from Florida State University, Tallahassee, USA, in 2012.

He was a Graduate Research Assistant under the supervision of Prof. David A. Cartes with the Center for Advanced Power Systems (CAPS), where he was involved in research of power quality, especially active power filters. He was a Research Engineer at the State Grid Electric Power Research Institute. From May 2013, he was a Postdoctoral Fellow at the University of Alberta, Edmonton, AB, Canada, under the supervision of Prof. John Salmon, where he was engaged in power electronics, especially induction motor drives. In October 2014, he joined the Petroleum Institute, Abu Dhabi, UAE, as a Research/Teaching Associate. His current research interests include renewable energy, power electronics, motor drives, power quality, and power system analysis.

A. R. N. M. Reaz Ul Haque received the B.Sc. degree in electrical and electronics engineering (EEE) from the Bangladesh University of Engineering and Technology (BUET), Dhaka, Bangladesh in 2002 and the M.Sc. degree in power systems from the University of New Brunswick (UNB), Fredericton, NB, Canada in 2005.

He was a Lecturer at the North South University (NSU), Bangladesh. He is currently Graduate Teaching and Research Assistant under the supervision of Prof. John Salmon at the University of Alberta, Edmonton, AB, Canada. His current research interests include motor drives, voltage balancing of hybrid vehicles, and multilevel converters.

Nirmana Perera received the B.Sc. degree in electrical and electronic engineering from the University of Peradeniya, Peradeniya, Sri Lanka, in 2011, and the M.Sc. degree in power electronics/energy systems from the University of Alberta, Edmonton, AB, Canada, in 2015.

He was a Temporary Instructor till 2012 at the University of Peradeniya. In 2013, was a Graduate Research Assistant under the supervision of Prof. John Salmon at the University of Alberta. He is currently a Lecturer in the Department of Electrical and Electronic Engineering, University of Peradeniya, Sri Lanka. His current research interests include power electronic topologies, PWM schemes, drive systems, and fundamental physics of electricity and magnetism.

Andrew M. Knight (S'95–A'98–M'99–SM'06) received the B.A. degree in electrical and information sciences and the Ph.D. degree in electrical engineering both from the University of Cambridge, Cambridge, U.K., in 1994 and 1998, respectively.

He joined the University of Alberta as an Assistant Professor in 1999 and rose to the rank of Professor. In 2013, he joined the Department of Electrical and Computer Engineering, University of Calgary, Calgary, AB, Canada, as a Professor and Transmission Electric Industry Chair. His current research interests include efficient utilization of electrical energy, including transmission, energy conversion, and storage, and aspects related to increased penetration of renewable energy, distributed generation, and energy efficiency.

Dr. Knight is a Professional Engineer, registered in the Province of Alberta, Canada, a Chartered Engineer in the U.K. He is a recipient of an IEEE Power and Energy Society prize paper award and three prize paper awards from the IEEE Industry Applications Society. He is the Chair of the IEEE IAS Electric Machines Committee, a Member of the IEEE Smart Grid R&D Committee, the General Co-Chair of the IEEE ECCE 2015, the General Chair of the IEEE ECCE 2017, and the IAS Executive Board Member-at-Large.

John Salmon (S'86–M'86) received the B.Sc.Eng. degree from Imperial College London, London, U.K., in 1982, the M.Eng. degree from McGill University, Montreal, QC, Canada, in 1984, and the Ph.D. degree from Imperial College London, in 1987.

In 1987, he became an Assistant Professor in the Department of Electrical Engineering, University of Alberta, Edmonton, AB, Canada, where he has been a Full Professor since 1996. He has conducted industrially funded power-electronics research projects covering a wide range of applications, such as electronic ballasts for fluorescent lamps and metal-halide high-intensity discharge lamps, utility interface of micro turbine generators using high-speed permanent magnet generators, medium-voltage industrial drive systems, and soft starters for medium-voltage induction motors. His current research interests include industrial drive systems and their utility interface multipulse utility rectifiers, multilevel voltage-source converters, high-speed ac drive systems, coupled inductor inverters, floating bridge power electronics for motor control applications, battery voltage balancing networks, and multifunctional pulsewidth-modulated converters.

Dr. Salmon is a recent recipient of two prize paper awards from the IEEE Industry Applications Society: the first prize from the Industrial Drives Committee in 2008 and the first prize from the Industrial Power Converter Committee in 2009.